Duty-Ratio Control of Nonlinear Phase Noise in Dispersion-Managed WDM Transmissions Using RZ-DPSK Modulation at 10 Gb/s

A. Tonello, S. Wabnitz, *Member, IEEE, Member, OSA*, and O. Boyraz, *Member, IEEE*

***Abstract*—The authors compare analytical and numerical estimates, showing that the nonlinear phase noise of short optical pulses associated with the coupling between amplified spontaneous emission noise and fiber nonlinearity may be controlled by adjusting the duty cycle of the return-to-zero (RZ) signal modulation format. The impact of this effect in the optimization of the performance of 10-Gb/s dispersion-managed wavelength division multiplexed (WDM) systems using RZ-differential phase-shift keying (DPSK) modulation is discussed. By extensive numerical simulations, it is shown that the transmission quality of ultradense WDM systems using the RZ-DPSK modulation format may be significantly enhanced by optimizing the duty cycle of the RZ pulses.**

***Index Terms*—Nonlinear optics, optical fiber communication, phase modulation.**

I. Introduction

DIFFERENTIAL phase-shift keying (DPSK) modulation format has become a competitive choice for ultralong-haul (ULH) optical transmission systems due to a 3-dB improvement in receiver sensitivity when compared to ON–OFF-keying (OOK) formats [1]–[3]. While this improvement provides a great advantage of DPSK formats over the OOK formats as far as linear noise accumulation is concerned, the situation is more complex in the presence of nonlinear transmission penalties. Indeed, when considering ULH dense wavelength division multiplexed (DWDM) systems, the overall transmission performance is also limited by nonlinear effects such as interchannel cross-phase modulation (XPM) crosstalk, intrachannel four-wave mixing (IFWM) [4], and self-phase-modulation-induced nonlinear phase noise (NPN) [5]–[7]. Although the variance of NPN (or Gordon–Mollenauer [8] noise) grows larger with the cube of the total transmission distance, when using the DPSK format, one employs a continuous RZ-pulse train, which leads to significant reductions of both XPM and IFWM crosstalks. All in all, in a situation when the system performance is equally limited by linear [i.e., amplified spontaneous emission (ASE) noise] and nonlinear effects, the maximum reach of ULH systems using the DPSK format turns out to be generally greater than the corresponding reach of systems using the OOK format [2], [4], [5].

In this paper, we shall be mainly concerned with the possibility of controlling by means of optimally adjusting the input signal format, the detrimental action of NPN. For definiteness, we shall refer to the relevant case of a 10-Gb/s system using the RZ-DPSK modulation format. In the first part of this paper, we will present an approximate but analytical treatment of the statistical properties (i.e., variance) of the NPN of an isolated RZ pulse. The validity of our analytical approximation will be verified by comparing its predictions with the numerical simulations. As we shall see, this paper reveals that the variance of NPN in a dispersion-managed fiber-optics link may be substantially reduced by properly decreasing the duty cycle of an RZ pulse. From a physical point of view, this occurs because short pulses undergo rapid dispersive broadening, which reduces nonlinear phase shifts in the beginning of transmission spans. Therefore, a quasi-linear propagation regime (or "pulse overlap transmission") is achieved [9]. We will also show that an NPN-variance reduction by decreasing the signal duty cycle is observed when performing numerical simulations involving a relatively long (256) RZ-pulse sequence. Note that, owing to the presence of the fiber chromatic dispersion, the phase jitter of the output pulses is accompanied by significant amplitude jitter as well. Of course, the overall system performance will be affected by both phase and amplitude jitters. We have also confirmed that the dominant nonlinear penalty for our 10-Gb/s single-channel-transmission-examples results from the coupling between signal and ASE noise and not from nonlinear intrachannel effects such as IFWM.

In Section II of this paper, we shall compare our theoretical predictions with the results of extensive numerical simulations, which confirm the predicted transmission improvement of single-channel 10-Gb/s RZ-DPSK transmissions by means of reducing the signal duty cycle [10]. When considering a WDM system with tightly spaced channels, the duty cycle can only be reduced up to the point where interchannel crosstalks become the dominant penalty. Our numerical simulations of the performance of DWDM 10-Gb/s RZ-DPSK transmissions show that, for densely packed channels, the optimal duty cycle should be determined as a tradeoff between intrachannel NPN reduction and control of interchannel crosstalk.

Manuscript received March 2, 2006; revised June 10, 2006.

A. Tonello and S. Wabnitz are with the Laboratoire de Physique, Université de Bourgogne UMR National Center for Scientific Research (CNRS) 5027, 21078 Dijon-Cedex, France (e-mail: Alessandro.Tonello@u-bourgogne.fr; Stefan.Wabnitz@u-bourgogne.fr).

O. Boyraz is with the Department of Electrical Engineering and Computer Science, University of California, Irvine, CA 92697-2625 USA (e-mail: oboyraz@uci.edu).

Color versions of all figures are available online at http://ieeexplore.ieee.org.
Digital Object Identifier 10.1109/JLT.2006.882238

Note that earlier work has predicted that an improvement of the performance of OOK systems can be achieved by means of properly adjusting the duty cycle of the RZ pulses [11], [12]. In spite of the strong current interest in the RZ-DPSK-based transmissions, to date, the role of adjusting the pulse duty ratio has not been investigated for this modulation format. This paper intends to fill this gap: Indeed, we shall demonstrate that for DPSK systems, the proper optimization of pulse duty cycle may lead to much larger nonlinear penalty reductions than with systems using OOK formats. In order to estimate the system performance and compare its value with different duty ratios, we shall use the commercial simulation-software Virtual Photonics Transmission Maker 5.5 (VPTM). Moreover, as a metric of transmission performance, we shall adopt the usual definition of the Q factor as obtained from a single-ended DPSK receiver. When comparing the predictions of optimal-system operation that are obtained with this definition of the Q factor with the results obtained from direct bit error rate (BER) measurements in DPSK transmission experiments, other definitions of the Q factor (such as the so-called differential phase Q [7]) may be more appropriate to DPSK systems. Therefore, we added a last section devoted to the discussion of the validation of the duty-cycle dependence of standard monomode fiber (SMF)-based 10-Gb/s DPSK transmissions when using these different quality metrics.

II. Duty-Cycle Dependence of NPN

We shall discuss the effect of signal duty ratio on NPN variance by considering first the case of an isolated RZ pulse. In order to analytically compute the NPN variance, one may apply the variational method as first outlined in [13]. This method allows for the prediction of the evolution of the phase-noise variance as well as the usual basic pulse parameters like amplitude and chirp along any dispersion-managed link. The basic assumption behind the variational method is that the pulse temporal shape can be represented at all positions by a chirped Gaussian function. We refer to the Appendix for more details on the application of the variational method to the computation of the NPN variance (see also [13]).

For definiteness, let us consider the specific example of a dispersion-managed link comprising 30 identical spans of 70 km of SMF with a group velocity-dispersion (GVD) $D_{\mathrm{SMF}} = 17$ ps/km/nm and an effective cross section for the guided mode of 80 μm^2. After each span, we inserted a dispersion compensating fiber (DCF) module. We fixed the DCF length to 11 km, with the effective cross section of 20 μm^2. With the GVD $D_{\mathrm{DCF}} = -103$ ps/km/nm, we compensate 95% of the SMF span cumulated GVD. The numerical study of the next section will show that this specific choice of span compensation corresponds to the average system performance (as measured in terms of the quality Q factor at a single-end DPSK receiver) whenever the span compensation is varied across the 100% value.

Following the DCF module, an erbium-doped fiber amplifiers (EDFA) with 5-dB noise figure (NF) is inserted in order to compensate for span losses. We also included adjustable pre- and postchirp sections at the link input and output, respectively.

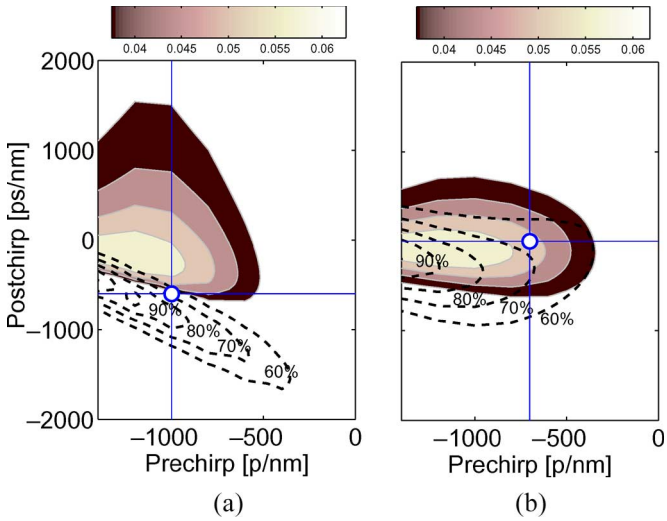

Fig. 1. Contour levels for analytical output (i.e., after 30 × 70 km spans or 2100 km) pulse peak power (dashed curves) and NPN (gray levels) with (a) 30% duty cycle and (b) 50% duty cycle. White circles identify the optimal (i.e., maximum Q) prechirp/postchirp combination when transmitting a sequence of bits.

We shall also restrict our attention to the data rate of 10-Gb/s per channel.

Let us consider the properties of individual Gaussian pulses and their NPN variance as they emerge at the output of a link composed by 30 SMF spans (i.e., a total transmission distance of 2100 km). We shall also fix the input-pulse energy to 200 fJ; for pseudorandom bit sequences, this corresponds to an average power of 0 dBm (3 dBm) for the OOK (DPSK) format. Fig. 1 compares the dependence of the output-pulse peak power and NPN variance on both pre- and postchirp for either short [30%, Fig. 1(a)] and long [50%, Fig. 1(b)] duty cycles. In Fig. 1, the dashed curves represent contour levels of the output-pulse peak power, normalized to its maximum value (over the whole scan of pre- and postchirp values). The different dashed curves in Fig. 1 thus indicate the pre- and postchirp combinations that reduce the output peak power down to 90%, 80%, 70%, and 60% of its maximum value, whereas the gray levels in Fig. 1 show the dependence on pre- and postchirp of the actual output NPN variance in radians (see the gray chart).

Fig. 1(a) shows that for small duty cycles (or short 30-ps pulses), the region of high peak-power levels (which corresponds to a compression of the output pulse to its original time width) is well separated from the region of largest NPN variances. On the other hand, Fig. 1(b) shows that in the case of relatively large duty cycles (or long 50-ps pulses), the region of highest output peak powers overlaps well with the region of largest NPN variances. Let us suppose now that the pre- and postchirp combination is selected in a manner such as to choose the maximum output peak power (which corresponds to optimal compensation of pulse broadening originating from the dispersion and self-phase modulation that are accumulated along the link) in both plots of Fig. 1. In this case, it is clear from Fig. 1 that reducing the RZ signal duty cycle from 50% down to 30% significantly decreases the NPN variance at the previously defined operating point. Note that, in a practical system, not every combination of pre- and postchirp can be

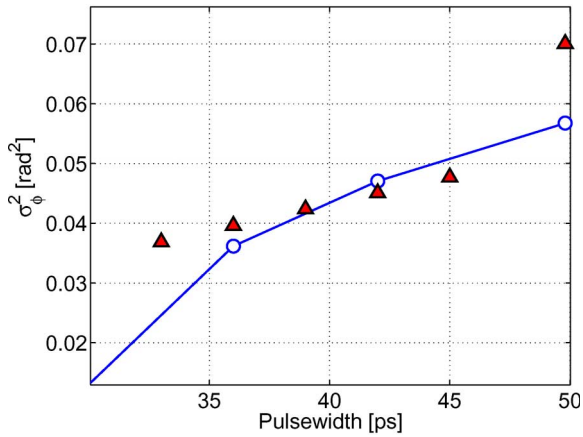

Fig. 2. Phase-noise variance versus pulsewidth. Solid line: Variation results. Triangles: Numerical variance as obtained from a set of 100 simulations.

selectable in order to obtain a desired received eye opening. For example, in a WDM transmission, it is possible to perform a per-channel optimization of the postchirp, whereas one cannot perform a per-channel optimization of the prechirp.

We could confirm that the statistical predictions of the variational method are in relatively good quantitative agreement with Monte Carlo numerical simulations of the propagation of a single Gaussian pulse, as obtained by using a beam propagation method (BPM). We used the same pulse energy as in Fig. 1, and we considered a transmission distance of 2100 km while keeping the span-compensation ratio of 95%. We took an EDFA NF of 5 dB, and we transmitted many times the same pulse with different random noise realizations. Indeed, in Fig. 2, we compare the analytical estimation (solid curve and empty dots) with the numerical evaluation (triangles) of the dependence of the NPN variance upon the input-pulse width (or duty cycle). The numerical NPN variance was obtained from an ensemble average of 100 simulations (with different noise seeds) for each couple of pre- and postchirp values. In Fig. 2, we selected the variational NPN corresponding to the pre- and postchirp pair that yields the highest received peak power (as discussed with reference to Fig. 1). Similarly, the NPN variance of BPM single-pulse-transmission simulations was calculated for precisely the pre- and postchirp values that yield the highest output peak power. Note from Fig. 2 that a discrepancy is observed between variation analysis and numerical simulations whenever the cumulated noise is very small, that is, for pulsewidths below 35 ps. For this reason, we did not plot the variation results (solid curve) for pulse durations below the 30-ps value.

Of course, the above-discussed analysis of the dynamics and phase-noise statistics of a single isolated pulse is not sufficient to fully predict the optimal-system performance. Indeed, in actual simulations, optimal pre- and postchirp values are chosen in a way such as to minimize all penalties, including those originating from both self-phase modulation as well as cross interactions. In other words, finding the optimal pre- and postchirp values involves simulating the transmission of relatively long (typically 256) bit sequences and evaluating the resulting transmission quality by means of estimators such as the Personick's Q factor.

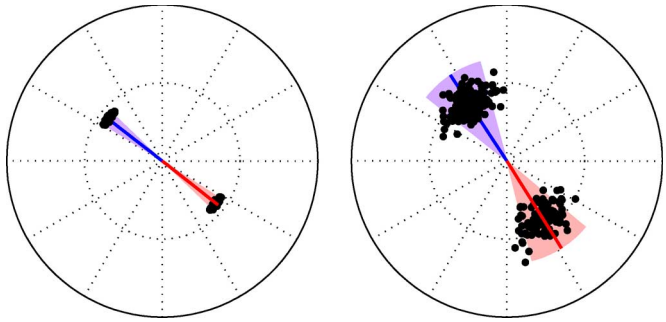

Fig. 3. Phasor diagram of a 256 pulse numerical transmission: 30-ps pulsewidth. Left: With noiseless amplification and ASE noise linearly added at the end of the transmission. Right: With noisy amplifiers.

We have therefore extended our study of the duty-cycle dependence of the NPN by performing a series of numerical simulations involving the transmission of a relatively long sequence of symbols. We considered a continuous sequence of 256 consecutive marks: The phase of each such pulse is either set to zero or π so that these two equal probability phase values form an uncorrelated random sequence. For a given pseudorandom sequence of phase alternations, we scanned the same wide range of pre- and postchirp values, as shown in Fig. 1. In order to measure the Q factor, we detected the output optical signal with the help of an interferometer including a 1-bit delay line. We detected the output of the destructive port of the interferometer, and we passed the electrical signal through a baseband 7-GHz fifth-order Bessel filter. The optimization of the resulting Q factor permitted us to identify the best pre- and postchirp values for a 10-Gb/s DPSK single-channel transmission. Let us restrict our attention now to the optimal pre- and postchirp values as they have been selected by means of the above procedure. For this configuration, we measured the complex value of the optical field envelope (before detection) at the center of the time slot of each pulse in the whole 256-bit sequence. Each of these measured field pulses has been classified in one of two sets, corresponding to their relative input phase (0 or π).

In the plot of Fig. 3(a), we show the Fresnel phase diagram of the 256 transmitted pulses with 30-ps duration. Here, the shaded area indicates three times the phase standard deviations $3\sigma_0$ or $3\sigma_\pi$, respectively. The comparison between the two plots in Fig. 3(a) and (b) permits us to discriminate between deterministic nonlinear signal degradations and jitters induced by coupling between the signal and the ASE noise. Indeed, in Fig. 3(a), we show the same phase diagram that is obtained with noiseless amplifiers, whereas the total ASE noise accumulated in the link is added to the signal right before the detection unit, whereas Fig. 3(b) shows the corresponding output signal phase diagram, as it is obtained by adding ASE noise to the signal at each amplifier site throughout the link. By comparing Fig. 3(a) and (b), it is clear that the dominant contribution to amplitude and phase jitter is due to ASE-signal coupling and not deterministic signal degradation such as intrachannel XPM or IFWM.

In order to elucidate the role of signal-format duty cycle on the balance between deterministic and ASE-noise-induced jitters, in Fig. 4, we have reproduced the plots of Fig. 3, but we

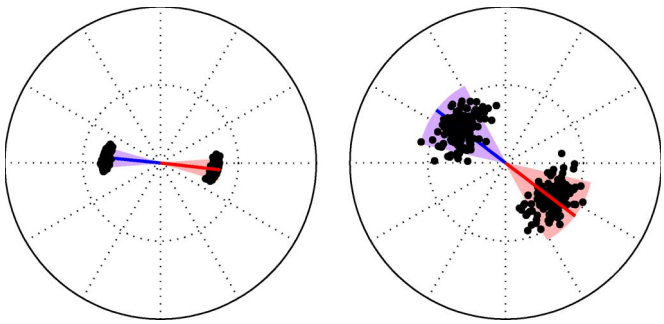

Fig. 4. Phasor diagram of a 256-pulse numerical transmission: 50-ps pulsewidth. Left: With noiseless amplification and ASE noise linearly added at the end of the transmission. Right: With noisy amplifiers.

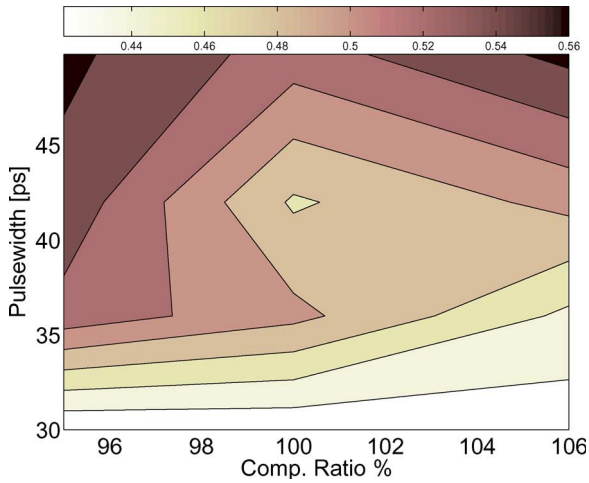

Fig. 5. Sum of standard deviations $\sigma_0 + \sigma_\pi$ versus pulsewidth and compensation ratio.

use input 50-ps pulses (50% duty cycle). The plots in Fig. 4(a) and (b) have been obtained by recalculating the optimal pre- and postchirp pair for the case of 50% duty cycle. By comparing the results of Figs. 3 and 4, it is clear that increasing the duty cycle from 30% to 50% leads to a significant growth of both output amplitude and phase variances in a manner similar to the case of single pulse transmission. Note from Figs. 3(b) and 4(b) that the significant amplitude jitter that is coupled to phase jitter by the chromatic dispersion of the fibers.

Let us finally explore the role of both signal format and average link dispersion on the output NPN variance. In Fig. 5, we plot the dependence of the sum of the two-phase variances $\sigma_0 + \sigma_\pi$ upon both signal-pulse width (duty cycle) and span-compensation ratio. As can be seen, the signal phase variance grows larger as the duty cycle is increased from 30% to 50%. Fig. 5 shows that this effect is more significant in the case of an undercompensated link. Moreover, Fig. 5 also shows that with short (around 30 ps) pulses, the phase variance is nearly independent of the compensation ratio (albeit with a slight NPN-variance reduction in the case of an overcompensated link).

The combined analytical and numerical results of this section show that the control and minimization of the NPN variance does require a careful adjustment of both the signal-format duty cycle as well as the dispersion map (pre- and postchirp, span-compensation ratio). So far, we considered the case of

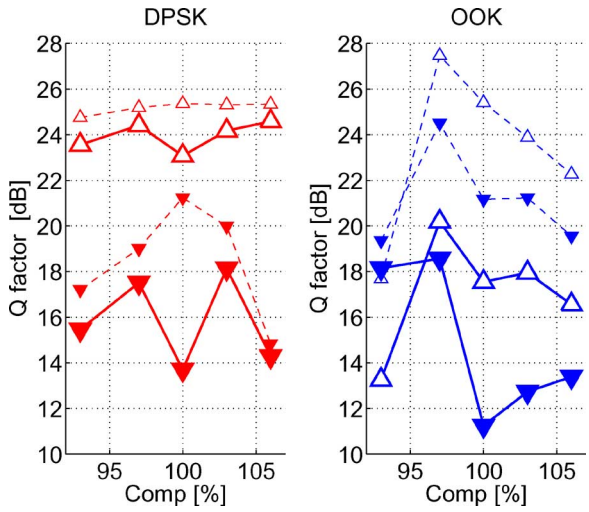

Fig. 6. Output system performance versus span-compensation ratio for DPSK and OOK systems for single-channel (dashed curves) and WDM (solid curves) transmission and 50% (filled triangles) or 30% (empty triangles) duty ratios.

PSK format-based transmission systems. As we shall see in detail in the next section, whenever an OOK format is employed, pulse-to-pulse (or intrachannel) interactions become a more significant source of penalty, which will lead to the preferential choice of slightly undercompensated spans [14].

III. Numerical Optimization of OOK and DPSK Formats

As we shall see in this section, the analytical predictions of Section II turn out to be in good qualitative and quantitative agreement with the single-channel numerical simulation results of both OOK and DPSK transmissions. We measured the system performance in terms of the Q factor with a single-ended detection scheme. In this case, and in the limit of an ASE noise-limited system, system performance using either OOK or DPSK modulation format is expected to be about the same [15], [16]. Note that the important advantage of the DPSK format, which is provided by the 3-dB enhancement in receiver sensitivity, can be only reached when using a balanced detection scheme. However, such 3-dB improvement would not be visible by simply calculating the Q factor from a set of numerical simulations [15], [16]. In the numerical modeling, we have employed the Virtual Photonics Transmission Maker 5.5 commercial software package, with five identical 128-bit pseudo random bit sequences (PRBSs) in each channel before the prechirp fiber module, whereas the EDFA ASE noise sequence was kept the same as we changed the input-pulse duty cycle as well as the other system and map parameters.

Fig. 6 illustrates the dependence of the output (at the total transmission distance of 2100 km) Q factor upon span-compensation ratio, in the case of systems using either RZ-DPSK (Fig. 6, left) or RZ-OOK (Fig. 6, right) modulation format. Moreover, in Fig. 6, we compare the results of simulations for two different values of the duty cycle of the RZ pulses. The Q factor of the central channel (out of a comb of five channels with 50-GHz spacing) was obtained by independently optimizing both pre- and postchirp, whereas the

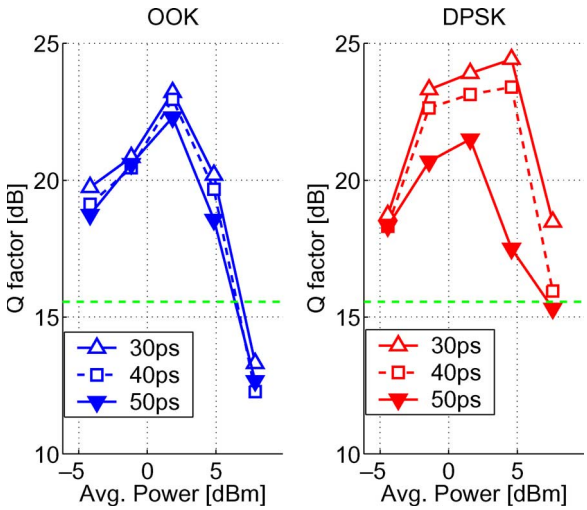

Fig. 7. System performance versus input power for OOK and DPSK WDM transmission with 97% span compensation and different duty cycles. Dashed horizontal lines indicate $Q = 16$ dB.

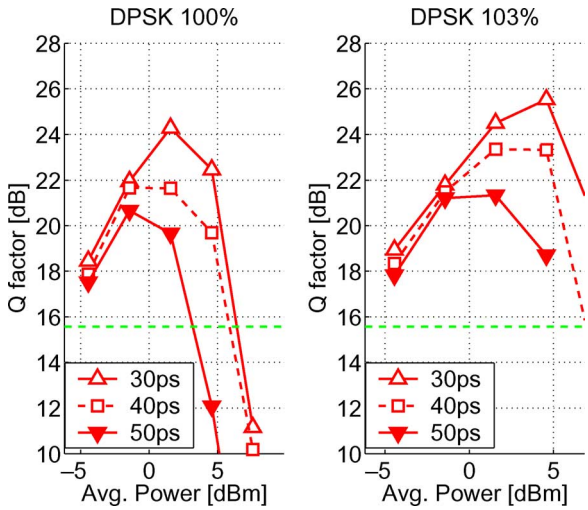

Fig. 8. System performance versus input power for a DPSK WDM transmission with 100% or 103% span compensation and different duty cycles.

input power was fixed to 4.6 dBm. In Fig. 6, the empty (filled) triangles correspond to the case of 30 ps (50 ps) RZ pulses. Moreover, in Fig. 6, the dashed and solid curves indicate either single channel or DWDM transmissions (with 50-GHz channel spacing). As can be seen in Fig. 6, in the case of 97% per-span compensation (i.e., with slightly undercompensated SMF spans) for both single channel and WDM DPSK transmissions, a 6-dBQ performance improvement is achieved by reducing the pulsewidth from 50 to 30 ps (i.e., by reducing the duty cycle from 50% to 30%). On the other hand, Fig. 6 also shows that the same duty-cycle reduction from 50% to 30% only yields 2-dBQ improvement whenever the OOK modulation format is used.

The above results indicate that the observed strong dependence of the output system performance upon the adjustment of the duty ratio is a peculiar property of the DPSK modulation format. Fig. 6 also shows that the XPM crosstalk leads to more than 7 dBQ of penalty whenever the OOK format is used, whereas WDM interchannel crosstalk is virtually absent with the 10-Gb/s DPSK format and 50-GHz channel separation as long as per-span GVD compensation detuned from the 100% (worst case) value, in agreement with the experimental observations by Xu *et al.* [2]. Another remarkable result of Fig. 6 is that, for a fixed value of the duty ratio, the single-channel performance with the OOK format is more sensitive to the precise value of the inline compensation ratio than with the DPSK modulation format. Moreover, in agreement with the analytical predictions of Section II, the RZ-OOK format works better with an undercompensated (i.e., $< 100\%$) span. In contrast, Fig. 6 shows that the DPSK format shows a slightly better performance with overcompensated ($> 100\%$) spans. These results well agree with the predictions of Section II. Note that the large (i.e., > 25) Q values in Fig. 6 and elsewhere in this paper are simply meant as an indication that for that specific choice of parameters, the nonlinear and dispersive impairments that are included in our simulations do not affect the error-free system performance.

Let us consider next a more detailed comparison of the duty-cycle dependence of both RZ-OOK and RZ-DPSK DWDM 10-Gb/s transmissions with 50-GHz channel spacing. Fig. 7 depicts the dependence of the output Q factor on input signal power for RZ-OOK and RZ-DPSK modulation formats, with three different values (i.e., 30%, 40%, and 50%) of the duty cycle, and an undercompensated (97%) dispersion map. Whereas, Fig. 8 shows the results of DWDM RZ-DPSK transmissions only, with either fully compensated (100%) or overcompensated (103%) maps. Note that 3% overcompensation of the 70-km SMF span amounts to 35.7 ps/nm. In each case, system performance was optimized by scanning over a set of pre- and postchirp values.

As can be seen from Fig. 7, with the RZ-OOK format, the output Q factor is only marginally affected (i.e., less than 1-dBQ variation) by the adjustment of the duty cycle from 30% to 50%, whereas with the RZ-DPSK format, the system performance can be improved by as much as 7–10 dBQ at relatively high input powers ($\sim$5 dBm) by reducing the duty cycle from 50% to 30%. Additionally, Figs. 6–8 show that for any value of the duty cycle, the WDM system performance is markedly improved for both OOK and DPSK systems with either under- or overcompensation. Indeed, 100% span dispersion compensation is accompanied by strong XPM and IFWM crosstalks. Finally, Figs. 6–8 confirm that overcompensation by 103% is the optimal choice for the DPSK format.

In WDM transmissions, optimal RZ-pulse width results in a tradeoff between intrachannel effects such as IFWM, NPN, and interchannel crosstalk. For that reason, we numerically compared the duty-cycle dependence of the RZ-DPSK system performance with two different values of the WDM channel spacing, namely 50 GHz (Fig. 9 top) and 25 GHz (Fig. 9 bottom). In each case, Fig. 9 displays the overall system performance when using the DPSK format (with 97% span compensation) as a function of RZ-pulse width for two different values of the input power [namely, 1.6 dBm (Fig. 9, filled dots) or 4.6 dBm (Fig. 9, empty dots)].

Fig. 9 (top) shows that with 50-GHz channel spacing, the optimum duty cycle is equal to 20%. Such optimal duty cycle

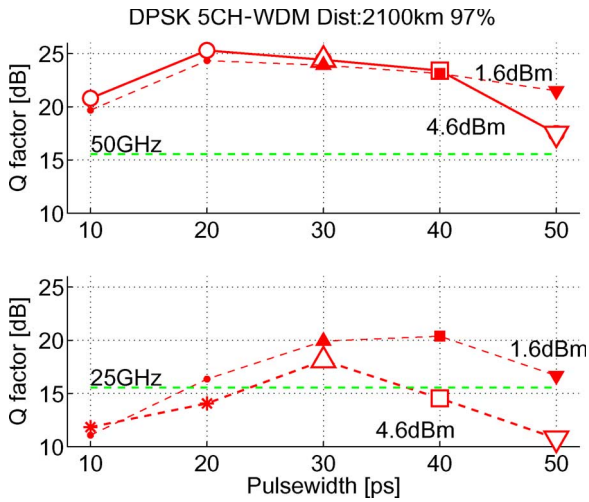

Fig. 9. System performance versus input-pulse width for DPSK WDM transmission with 97% span compensation, different input powers, and channel spacing of 50 GHz (top) or 25 GHz (bottom).

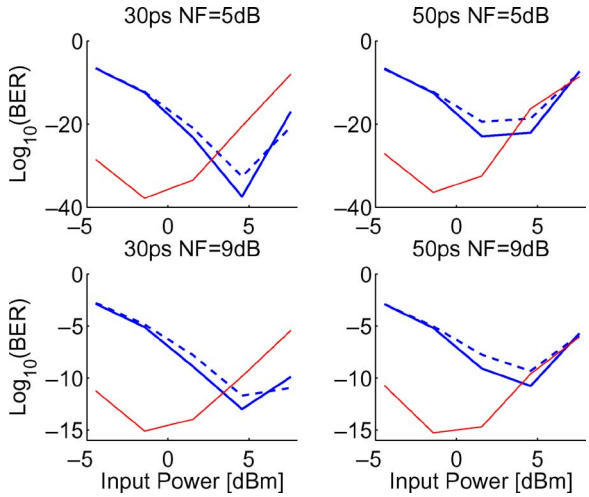

Fig. 10. BER versus input power for different pulse durations and EDFA NFs. Thick lines: BER obtained from the conventional Q factor (solid: Constructive port, dashed: Destructive port). Thin lines: BER from the phase Q factor as defined in [7].

is basically unchanged when increasing the channel power from 1.6 to 4.6 dBm, whereas Fig. 9 (bottom) shows that in a DWDM RZ-DPSK system with 25-GHz spacing, the optimal pulsewidth is strongly affected by interchannel crosstalks and by input signal power. As a result, in this case, the optimal duty cycle should be increased well above 20%. Indeed, Fig. 9 (bottom) shows that with 25-GHz channel spacing, the optimum duty cycle should be set in the range between 40% and 30%, which corresponds with the input-power levels that vary between 1.6 and 4.6 dBm, respectively.

IV. Simulation Validation

The layout of the DPSK transmitter that we used in our transmission-system simulations based on the VPTM commercial software was composed by an optical Gaussian pulse generator followed by a phase modulator driven by an electrical nonreturn to zero (NRZ) signal. The rise time of the modulator phase transitions was set to 25 ps. The NRZ electrical signal that drives the modulator phase transitions was obtained as usual from the logic XOR of a PRBS sequence. The signal-pulse duty cycle was varied by changing the optical pulsewidth value at the Gaussian pulse generator. The peak power of the input signal pulse was adjusted accordingly in order to keep unchanged the signal average power while adjusting its duty cycle (or optical pulse duration). For the generation of the OOK signal format, we used the same optical Gaussian pulse generator. It is important to relate the output Q factor of Figs. 6–9 with the output optical signal-to-noise ratio (OSNR). For example, in the case of an RZ-DPSK transmission with a 30-ps pulsewidth and the input peak power of 9 mW (i.e., 4.58-dBm input signal average power), after the propagation distance of 2100 km, the OSNR was equal to 24.4 dB (over the signal bandwidth of 12.5 GHz). The layout of our DPSK receiver included a flattop optical filter, a 1-bit delay line, and a photodetector with a 7.5-GHz electrical filter, and a clock recovery unit.

So far, we adopted the conventional definition of the Q factor as obtained from a single-ended DPSK detection scheme. It has been recently pointed out [7] that the evaluation of DPSK system performance (i.e., of the measured BER) based on such a quality metric may lead to invalid estimations of the optimal signal power level at the entry of the SMF spans. Indeed, in [7], it was shown that the Personick's Q factor as is calculated from the electrical signal that results from a balanced DPSK receiver overestimates the optimal signal input power by several decibels. In fact, Wei *et al.* [7] proposed a different formula for the Q factor that is directly based on the calculation of the phase-noise variance (see [7, eq. 2]). Note that in [7], the signal duty cycle was fixed at 33%.

In order to clarify this issue in the context of the SMF-based system under consideration here, we compared in Fig. 10 the relative offset among the results obtained from single-channel simulations with different duty cycles and performance metrics. The simulations of Fig. 10 were performed by using the fixed prechirp value of 900 ps/nm, the overall transmission distance of 2100 km, and the compensation ratio of 106% (with PRBS of 2048 bits). In Fig. 10, we compare the predictions of two different metrics for the BER evaluation. The first performance metric is the conventional Personick's or amplitude Q factor (thick lines), whereas the second metric corresponds to the differential-phase Q factor as obtained from [7, eq. 2] (thin lines). Fig. 10 shows the results obtained with either 30-ps (left column of all insets) or 50-ps RZ pulses (right column of all insets). Upper and lower insets in Fig. 10 correspond to different EDFA's NFs. Similar to the situation described in [7], in the case of input pulses of time width equal to 30 ps, we observed a considerable difference in the predictions of optimal signal power at the SMF input with the two definitions of the Q factor. On the other hand, for relatively high signal powers or with input pulses with a 50-ps duration, the BER values as obtained from both the amplitude or phase Q estimators show similar values. Fig. 10 also shows that the discrepancy among the BER values as obtained from the amplitude or phase Q metrics is significantly affected by the value of the duty cycle (note that in [7], the signal duty cycle was kept constant to

33%). Additionally, Fig. 10 shows that the benefits of a shorter duty cycle are more evident whenever the cumulated ASE noise is relatively low (that is, with the realistic value of the EDFA NF = 5 dB). On the other hand, enhancing the EDFA NF (up to 9 dB) as it may be required in order to directly compute the system errors as was done in [7] has the effect of attenuating the system impact of adjusting the input-pulse duration.

V. Conclusion

In summary, we predicted by an analytical treatment and confirmed by extensive numerical simulations that significant performance improvements of 10-Gb/s transmissions with the RZ-DPSK format may be obtained by properly reducing the RZ-pulse duty cycle. More specifically, we found that the optimal duty cycle is about 20% whenever intrachannel nonlinear penalties dominate (i.e., for 50-GHz channel spacing). With tight channel spacing (i.e., 25 GHz), we found that the presence of interchannel-crosstalk penalties leads to an increase of the optimal duty cycle of DWDM RZ-DPSK transmissions up to the 30%–40% range.

Appendix

Nonlinear pulse propagation in a dispersion-managed transmission link may be described in terms of the following nonlinear Schrödinger equation:

$$\frac{\partial q}{\partial z} = [g(z) - \alpha(z)]\, q - i\beta(z)\frac{\partial^2 q}{\partial t^2} + i\gamma(z)\,|q|^2\, q + R(z). \tag{A1}$$

By considering a Gaussian ansatz for the pulse shape, namely

$$q(z,t) = a \exp\left[i\phi - (1+iC)t^2/(2\tau^2)\right] \tag{A2}$$

one obtains by the variational method the following set of coupled ordinary differential equations (ODEs) for the parameters τ and C associated with the pulsewidth and chirp, respectively:

$$\begin{aligned}\frac{d\tau}{dz} &= \beta(z)\frac{C}{\tau}\\ \frac{dC}{dz} &= (1+C^2)\frac{\beta(z)}{\tau^2} + \gamma\frac{E}{\tau\sqrt{2\pi}}.\end{aligned} \tag{A3}$$

In the presence of ASE noise, the pulse parameters obey stochastic coupled ODEs, and one finds the following expressions for the evolution with distance Z of variances and cross variances of the various pulse parameters [12]:

$$\begin{aligned}\frac{d\langle\Delta E\Delta\tau\rangle}{dz} &= -2\nu\langle\Delta E\Delta c\rangle + \beta_1\langle\Delta E\Delta\phi\rangle + \sigma_{e\tau}\\ \frac{d\langle\Delta E\Delta c\rangle}{dz} &= \gamma\langle\Delta E\Delta\tau\rangle - (2\beta_2+\gamma)\langle\Delta E\Delta c\rangle\\ &\quad + 2\nu\langle\Delta E\Delta\phi\rangle + \sigma_{ec}\\ \frac{d\langle\Delta E\Delta\phi\rangle}{dz} &= \frac{5\gamma}{4}\langle\Delta E\Delta\tau\rangle - \left(\beta_1+\frac{5\gamma}{4}\right)\langle\Delta E\Delta c\rangle + \sigma_{e\phi}\\ \frac{d\langle\Delta\tau^2\rangle}{dz} &= -4\nu\langle\Delta\tau\Delta c\rangle + 2\beta_1\langle\Delta\tau\Delta\phi\rangle + \sigma_{\tau\tau}\\ \frac{d\langle\Delta\tau\Delta c\rangle}{dz} &= \gamma\langle\Delta E\Delta c\rangle - (2\beta_2+\gamma)\langle\Delta\tau\Delta c\rangle\\ &\quad + \beta_1\langle\Delta c\Delta\phi\rangle + \sigma_{\tau c}\\ \frac{d\langle\Delta\tau\Delta\phi\rangle}{dz} &= \frac{5\gamma}{4}\langle\Delta E\Delta c\rangle - \left(\beta_1+\frac{5\gamma}{4}\right)\langle\Delta\tau\Delta c\rangle\\ &\quad - 2\nu\langle\Delta c^2\rangle + \beta_1\langle\Delta\phi^2\rangle + \sigma_{\tau\phi}\\ \frac{d\langle\Delta c^2\rangle}{dz} &= 2\gamma\langle\Delta E\Delta\phi\rangle - 2(2\beta_2+\gamma)\langle\Delta\tau\Delta\phi\rangle\\ &\quad + 4\nu\langle\Delta c\Delta\phi\rangle + \sigma_{cc}\\ \frac{d\langle\Delta c\Delta\phi\rangle}{dz} &= \frac{5\gamma}{4}\langle\Delta E\Delta\phi\rangle + \gamma\langle\Delta\tau^2\rangle - \left(\beta_1+\frac{5\gamma}{4}\right)\langle\Delta\tau\Delta\phi\rangle\\ &\quad - (2\beta_2+\gamma)\langle\Delta c\Delta\phi\rangle + 2\nu\langle\Delta\phi^2\rangle + \sigma_{c\phi}\\ \frac{d\langle\Delta\phi^2\rangle}{dz} &= \frac{5\gamma}{4}\langle\Delta\tau^2\rangle - 2\left(\beta_1+\frac{5\gamma}{4}\right)\langle\Delta c\Delta\phi\rangle + \sigma_{\phi\phi}.\end{aligned}$$

References

[1] A. H. Gnauk, G. Raybon, S. Chandrasekhar, J. Leuthold, C. Doerr, L. Stulz, A. Agarwal, S. Banerjee, D. Grosz, S. Hunsche, A. Kung, A. Marhelyuk, D. Maywar, M. Movassaghi, X. Liu, C. Xu, X. Wei, and D. M. Gill, "2.5 Tb/s (64 × 42.7 Gb/s) transmission over 40 × 100 km NZDSF using RZ-DPSK format and all-Raman-amplified spans," in *Proc. OFC*, 2002, pp. FC2-1–FC2-3.

[2] C. Xu, X. Liu, L. F. Mollenauer, and X. Wei, "Comparison of return-to-zero differential phase-shift keying and ON–OFF keying in long-haul dispersion managed transmission," *IEEE Photon. Technol. Lett.*, vol. 15, no. 4, pp. 617–619, Apr. 2003.

[3] T. Mizuochi, K. Ishida, T. Kobayashi, J. Abe, K. Kinjo, K. Motoshima, and K. Kasahara, "A comparative study of DPSK and OOK WDM transmission over transoceanic distances and their performance degradations due to nonlinear phase noise," *J. Lightw. Technol.*, vol. 21, no. 9, pp. 1933–1943, Sep. 2003.

[4] X. Wei and X. Liu, "Analysis of intrachannel four-wave mixing in differential phase-shift keying transmission with large dispersion," *Opt. Lett.*, vol. 28, no. 23, pp. 2300–2302, Dec. 2003.

[5] J.-K. Rhee, D. Chowdhury, K. S. Cheng, and U. Gliese, "DPSK 32 × 10 Gb/s Transmission modeling on 5 × 90 km terrestrial system," *IEEE Photon. Technol. Lett.*, vol. 12, no. 12, pp. 1627–1629, Dec. 2000.

[6] H. Kim and A. H. Gnauk, "Experimental investigation of the performance limitation of DPSK systems due to nonlinear phase noise," *IEEE Photon. Technol. Lett.*, vol. 15, no. 2, pp. 320–322, Feb. 2003.

[7] X. Wei, X. Liu, and C. Xu, "Numerical simulation of the SPM penalty in a 10-Gb/s RZ-DPSK system," *IEEE Photon. Technol. Lett.*, vol. 15, no. 11, pp. 1636–1638, Nov. 2003.

[8] J. P. Gordon and L. F. Mollenauer, "Phase noise in photonics communications systems using linear amplifiers," *Opt. Lett.*, vol. 15, no. 23, pp. 1351–1353, Dec. 1990.

[9] X. Liu, C. Xu, and X. Wei, "Nonlinear phase noise in pulse-overlapped transmission based on return-to-zero differential phase-shift-keying," presented at the Eur. Conf. Optical Commun. (ECOC), Copenhagen, Denmark, 2002, Paper 9.6.5.

[10] A. Tonello, S. Wabnitz, and O. Boyraz, "Duty ratio control of nonlinear phase noise in dispersion managed WDM systems using RZ-DPSK modulation," presented at the Optical Fiber Commun. Conf. (OFC), Anaheim, CA, 2005, Paper OME55.

[11] H. Maeda, M. Murakami, N. Ohkawa, and T. Imai, "Optimization of signal pulse duty factor in long-distance optical amplifier systems," *IEEE Photon. Technol. Lett.*, vol. 10, no. 8, pp. 1183–1185, Aug. 1998.

[12] D. Kovsh, E. A. Golovchenko, and A. N. Pilipetskii, "Enhancement in performance of long-haul DWDM systems via optimization of the transmission format," in *Proc. Optical Fiber Commun. (OFC)*, Anaheim, CA, 2002.

[13] C. J. McKinstrie, C. Xie, and T. I. Lakoba, "Efficient modelling of phase jitter in dispersion managed soliton systems," *Opt. Lett.*, vol. 27, no. 21, pp. 1887–1889, Nov. 2002.
[14] T. Inoue, H. Sugahara, A. Maruta, and Y. Kodama, "Interactions between dispersion managed solitons in optical-time-division-multiplexed systems," *IEEE Photon. Technol. Lett.*, vol. 12, no. 3, pp. 299–301, Mar. 2000.
[15] X. Zhang, G. Zhang, C. Xie, and L. Wang, "Noise statistics in optically preamplified differential phase-shift keying receivers with Mach–Zehnder interferometer demodulation," *Opt. Lett.*, vol. 29, no. 4, pp. 337–339, Feb. 2004.
[16] ——, "Erratum to Noise statistics in optically preamplified differential phase-shift keying receivers with Mach–Zehnder interferometer demodulation," *Opt. Lett.*, vol. 30, no. 6, p. 676, Mar. 2005.

A. Tonello received the Laurea and Ph.D. degrees in electronics engineering from the University of Padova, Padova, Italy, in 1997 and 2001, respectively.

From 2001 to 2002, he was a Postdoc with the University of Trento, Trento, Italy. From 2002 to 2003, he was a Postdoc with the University of Padova. From 2003 to July 2006, he was a Postdoc with the Université de Bourgogne, Dijon, France. Currently, he is a Researcher with the Xlim Institute, University of Limoges, Limoges, France. His research concentrates on nonlinear effects in fibers and fiber-optic transmission systems. His research interests include statistical optics, numerical modeling of microstructured fibers, parametric effects, and supercontinuum generation. He is the author or coauthor of over 50 referred papers and conference presentations.

S. Wabnitz (M'03) received the Laurea degree in electronics engineering from the University of Rome "La Sapienza," Rome, Italy, the M.S. degree in electrical engineering from the California Institute of Technology (Caltech), Pasadena, and the Ph.D. degree in applied electromagnetism from the Italian Ministry of Education, Rome.

He has been a Researcher with the Optical Communications Department, the Ugo Bordoni Foundation, between 1985 and 1996, where he has contributed the theory of nonlinear wave propagation in optical fibers and waveguides, with particular interest in wave instabilities and soliton phenomena. In 1996, he became a Full Professor in physics with the Université de Bourgogne, Dijon, France. Between 1999 and 2003, he was on leave from the University to carry out research and development in the telecommunication industry. He spent two years working on optical soliton effects for submarine system applications at the Alcatel Research and Innovation Laboratory, Marcoussis, France, and two years as Manager of the Advanced Technology Group, Xtera Communications, Allen, TX. His current research activities involve nonlinear propagation effects in high-bit-rate optical communication systems and in photonic crystal structures. He is the author and coauthor of over 350 refereed papers and conference presentations.

Dr. Wabnitz is a member of the Optical Society of America and of the IEEE Laser and Electro-Optics Society.

O. Boyraz (M'96) received the B.S. degree from Hacettepe University, Ankara, Turkey, in 1993 and the M.S. and Ph.D. degrees from the University of Michigan, Ann Arbor, in 1997 and 2001, respectively, all in electrical engineering.

From 2001 to 2003, he was R&D Engineer with Xtera Communications, Allen, TX. From 2003 to 2005, he was a Postdoctoral Research Fellow with the Department of Electrical Engineering, University of California, Los Angeles. In August 2005, he joined the Department of Electrical Engineering and Computer Science, University of California, Irvine, as an Assistant Professor. He is the author or coauthor of more than 60 scientific publications and is the holder of three U.S. patents.

Dr. Boyraz is a member of the IEEE Laser and Electro-Optics Society.